01 Oct 2009

Current Sensing for Automotive Electronics -- A Survey

Asha Patel

Mehdi Ferdowsi
Missouri University of Science and Technology, ferdowsi@mst.edu

Recommended Citation

A. Patel and M. Ferdowsi, "Current Sensing for Automotive Electronics -- A Survey," *IEEE Transactions on Vehicular Technology*, vol. 58, no. 8, pp. 4108-4119, Institute of Electrical and Electronics Engineers (IEEE), Oct 2009.
The definitive version is available at https://doi.org/10.1109/TVT.2009.2022081

Current Sensing for Automotive Electronics—A Survey

Asha Patel and Mehdi Ferdowsi, *Member, IEEE*

***Abstract*—Current sensing is widely used in power electronic applications such as dc–dc power converters and adjustable-speed motor drives. Such power converters are the basic building blocks of drivetrains in electric, hybrid, and plug-in hybrid electric vehicles. The performance and control of such vehicles depend on the accuracy, bandwidth, and efficiency of its sensors. Various current-sensing techniques based on different physical effects such as Faraday's induction law, Ohm's law, Lorentz force law, the magnetoresistance effect, and the magnetic saturation effect are described in this paper. Each technique is reviewed and examined. The current measurement methods are compared and analyzed based on their losslessness, simplicity, and ease of implementation.**

***Index Terms*—Automotive electronics, current sensing, power electronics.**

I. Introduction

CURRENT measurement is required for control, protection, monitoring, and power-management purposes in automotive applications. Examples include control of motor drives [1], converter control [2]–[8], overcurrent protection [9], and state-of-the-charge estimation of batteries [10], [11]. Current measurement is intrusive as there is a need to insert some type of sensor. There are several other issues related to current sensing, such as ac or dc measurements, complexity, linearity, sensitivity to noise, isolation requirements, accuracy, stability, robustness, bandwidth, transient response, cost, and power loss. In addition, depending on the application, the average, peak, root mean square, or total waveform of the current signal needs to be measured. Most of the current measurement approaches can be categorized as a resistive- or an electromagnetic-based technique.

In resistive-based current-sensing techniques, the voltage drop across a sensing resistor is sensed to determine the current. Adding an external resistor to measure current [12]–[17] is acceptable where power loss, low bandwidth, noise, and nonisolated measurement are acceptable. Instead of adding an external sense resistor, several approaches use the internal resistance of the switches [18]–[20] or the inductor of the power electronic converter to measure the current [21]. These techniques are not involved with any extra power losses. However, they are not accurate, as the values of the discrete elements of the circuit are unknown. In addition to this, the technique that uses the internal resistance of an inductor for current sensing suffers from time-constant mismatching issues. Therefore, for an accurate and continuous current sensing, it is necessary for the time constants to be matched and that information about the off-chip elements is available. Current-sensing techniques with self-calibration and/or self-tuning are solutions to these problems [22]–[27]. In addition, average current-sensing techniques [6], [28], [29], which provide average current information, will also be discussed.

Electromagnetic-based current-sensing techniques are used to measure current in high-power applications where isolation is required. These techniques sense the magnetic field created by the current to be measured. Different current transformers (CTs) [30]–[39] are used to measure ac, dc, or pulsed current by coupling the secondary of a coil to the variable flux created by the primary current. Air-core-based CT techniques [29], [40]–[43] are used to measure ac or pulsed currents. Measurements by these techniques are insensitive to external magnetic perturbations. Current measurement techniques based on the Hall effect [44]–[56] are generally used to measure ac, dc, or complex currents with wide frequency bandwidths. Hall-effect-based sensors are more accurate than CTs, air core, and fiber-optic current sensors (FOCSs) [57]–[61]; however, they are more costly. Saturable inductor sensors [62] are used to provide high resolution, high accuracy, and faster speed. Magnetoresistor (MR) current sensors [63], [64] are used as alternatives to the Hall-effect-based techniques.

Different current-sensing methods applicable to automotive electronics such as resistive-based current sensing, electromagnetic-based current sensing, current sensing with self-tuning and/or autocalibration, and average current sensing are reviewed and evaluated in this paper. Different resistive- and electromagnetic-based current-sensing methods have been introduced, and their principles of operation are described in Sections II and III. Each method is evaluated based on the desired characteristics. Several measurement techniques have been compared with each other in Section IV. Section V draws conclusions and presents an overall evaluation of the current-sensing techniques.

II. Resistive-Based Current-Sensing Techniques

A. Using an Externally Added Sense Resistor

In Fig. 1, external sense resistor R_{sense} is placed in series with the inductor of a dc–dc buck power converter to measure

Manuscript received September 10, 2008; revised February 21, 2009. First published May 2, 2009; current version published October 2, 2009. This work was supported in part by the National Science Foundation under Grant 0640636. The review of this paper was coordinated by Prof. M. E. Benbouzid.

A. Patel is with the Dow Chemical Company, Houston, TX 77015-6544 USA (e-mail: apatel2@dow.com).

M. Ferdowsi is with the Department of Electrical and Computer Engineering, Missouri University of Science and Technology, Rolla, MO 65409 USA (e-mail: ferdowsi@mst.edu).

Digital Object Identifier 10.1109/TVT.2009.2022081

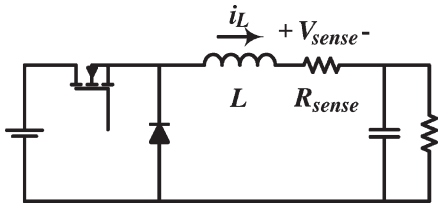

Fig. 1. Current sensing using an externally added sense resistor.

its current. $R_{\rm sense}$ functions as a current-to-voltage converter. Inductor current $i_L(t)$ is measured by sensing $V_{\rm sense}(t)$, which is the voltage across the sensing resistor, and is given by

$$i_L(t) = \frac{V_{\rm sense}(t)}{R_{\rm sense}}. \tag{1}$$

Discrete resistors or printed-circuit-board (PCB) traces are the most common methods of $R_{\rm sense}$ implementation [12]–[16]. High-precession $R_{\rm sense}$ guarantees accurate low-current measurements.

Due to its simplicity and accuracy, this method is used in applications such as power factor correction and overcurrent protection. The criteria for the selection of $R_{\rm sense}$ are voltage drop, accuracy, efficiency, power dissipation, parasitic inductance, and cost. The drawback of this technique is the power loss incurred by resistor $R_{\rm sense}$. Additionally, it does not provide measurement isolation from transient voltage potentials on the load. A noise filter is required to reduce the noise in the signal output, which will affect the overall system bandwidth. This technique is not applicable to high-performance dc–dc converters with efficiency requirements of more than 85%–90%.

A modified metal–oxide–semiconductor current-sensing technique using a current mirror to overcome power losses incurred by the sense resistor is presented in [17]. This method measures the current without requiring the entire output current to pass from the series sense resistor. This technique uses the microelectronic current mirroring concept. The current passing through the sense resistor is proportional to the output current, and its magnitude is smaller.

B. Using the Internal Resistance of an Inductor

To evade the use of an external sense resistor and its associated power losses, inductors in the topology of power converters can be used for current-sensing purposes, as shown in Fig. 2 [65]. Inductor L has an internal resistance of R_L and is magnetically coupled with an identical inductor (with equal number of turns).

The voltage across the main inductor terminals consists of V_1 and V_2, which can be described as

$$V_L = V_1 + V_2 = L\frac{di_L}{dt} + i_L R_L. \tag{2}$$

The extra winding with a minimum current loading is coupled with the main inductor, as shown in Fig. 2. The voltage across the extra winding is also V_1 due to the equal number of turns. If the voltages of both windings are subtracted, the resulting voltage is simply the $i_L R_L$ drop, which is proportional with the current to be measured. The disadvantage of this technique is that the measured current is sensitive to noise as V_2, which is the difference between two large voltages, is quite small. The inductor winding is built by copper wire; therefore, the temperature coefficient of copper's resistivity also applies. This method is appropriate for low-voltage high-current power converter applications.

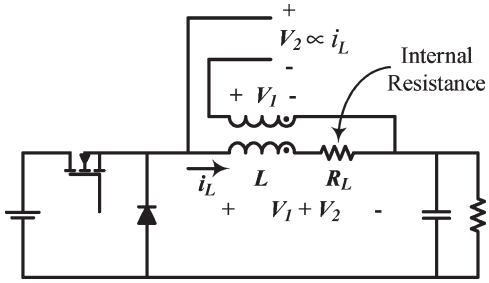

Fig. 2. Current sensing using the internal resistance of an inductor.

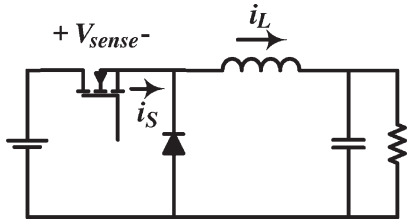

Fig. 3. R_{DS}-based current sensing.

C. Using the Internal Resistance of a MOSFET

A lossless current-sensing method based on the MOSFET drain–source resistance, which eliminates the need for external resistor $R_{\rm sense}$, is shown in Fig. 3 [18]–[20]. A MOSFET behaves like a resistor when it is turned on. This resistance R_{DS} can be described as

$$R_{DS} = \frac{l}{W\mu C_{\rm OX}(V_{GS} - V_T)} \tag{3}$$

where l is the channel length, W is the channel width, μ is the carrier mobility, $C_{\rm OX}$ is the gate oxide capacitance, and V_T is the threshold voltage. Therefore, it is possible to determine its current by measuring its drain–source voltage.

Current i_L can be determined by measuring switch current i_S (when the switch is conducting), which is given by

$$i_S = i_L = \frac{V_{\rm sense}}{R_{DS}}. \tag{4}$$

If needed, a sample-and-hold circuit is required to reconstruct the inductor current when the switch is not conducting. The value of resistance R_{DS} is provided in the MOSFET data sheet. The precession of this method depends on the accuracy of resistor R_{DS}. The data sheet gives only the maximum and typical values of resistor R_{DS}. The value of this resistance also depends on the temperature and gate drive voltage. This current-sensing method is very cost effective in low-voltage high-current point-of-load converters. Higher

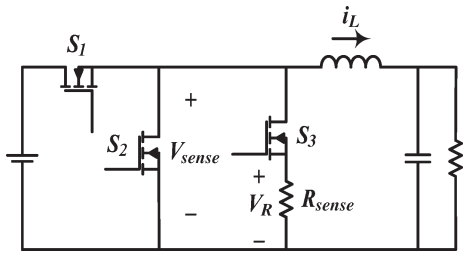

Fig. 4. MOSFET R_{DS}-based current-sensing technique with self-calibration.

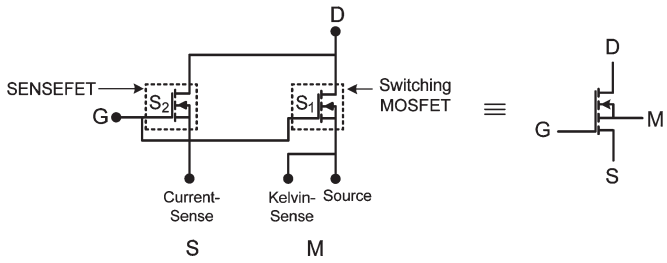

Fig. 5. Current-sensing power MOSFET.

switching frequencies and higher input voltages make this method inaccurate.

D. Using the Internal Resistance of a MOSFET With Real-Time Self-Calibration

The accuracy of most measurement techniques depends on some assumed parameter, e.g., the resistor value in resistive-based approaches. This assumed value is subject to temperature variations and inaccuracies. Due to these nonideal effects, conventional current measurement approaches are sensitive to temperature, tolerance of components, noise, and operating conditions. Therefore, self-calibration techniques are used to improve the losslessness, accuracy, and temperature variations of existing current measurement methods.

One approach combines an externally added sense-resistor technique with another lossless method, such as MOSFET R_{DS}- or filter-based current sensing for an accurate current measurement. In Fig. 4, an externally added sense resistor-based current-sensing method is combined with the MOSFET R_{DS}-based current sensing to effectively measure current i_L by determining the accurate value of resistance R_{DS} of switch S_2. Accuracy, along with losslessness, is achieved using an extra circuit, which is a series connection of switch S_3 and resistor $R_{\rm sense}$ [22], [23]. This extra circuit is infrequently added into the circuit for calibration purposes; therefore, the current rating of switch S_3 is small.

Considering a typical range for the duty ratio when it is not too close to 100%, during a normal cycle, inductor current i_L (when S_2 is on) is specified by

$$i_L = \frac{-V_{\rm sense}}{R_{DS}}. \tag{5}$$

Resistance R_{DS} is initially estimated from the MOSFET data sheet. To find the calibrated value of resistance $R_{DS}\,(R_{\rm DS\_cali})$, main switch S_2 is kept off, switch S_3 is turned on, and the voltage across resistor $R_{\rm sense}\,(V_R)$ is measured to find the value of current i_L, which is specified by

$$i_L = \frac{-V_R}{R_{\rm sense}}. \tag{6}$$

If current i_L is not affected by the switching of switch S_3, from (5) and (6), the calibrated value of R_{DS} can be described as

$$R_{\rm DS\_calib} = \frac{R_{\rm sense} * V_{\rm sense}}{V_R}. \tag{7}$$

The accuracy of (7) depends on the value of $R_{\rm sense}$. The combined resistance of switch S_3 and resistor $R_{\rm sense}$ must be low enough that the body diode of switch S_2 is not turned on when switch S_3 is conducting. Another concern when finding the value of $R_{\rm DS\_cali}$ is that the calibration cycle is performed only when the circuit is operating in the steady state. If these conditions are satisfied, then the value of (7) is used in place of resistance R_{DS} in (5) to accurately find current i_L.

E. Using a Current-Sensing Power MOSFET

Measuring electric currents using a current-sensing power MOSFET is more accurate than using the internal resistance of a MOSFET [66]–[74]. A power MOSFET consists of a large number of parallel-connected MOSFET cells. The gates, sources, and drains of all transistor cells are connected together. A current-sensing power MOSFET is structured, so that few cells in the power MOSFET are utilized to provide a sensing field-effect transistor (SENSEFET). The remaining MOSFET cells are used to provide the switching MOSFET. The current-sensing power MOSFET is a parallel connection of a SENSEFET (S_2) and a switching MOSFET (S_1), as shown in Fig. 5. Switch S_2 has relatively fewer transistor cells to provide a small sensing signal proportional to the switch S_1 current. An external sense resistor is placed on the scaled-down current to reduce the power dissipation; therefore, this technique is used to provide an accurate and lossless current measurement. A current-sensing power MOSFET is symbolically represented in Fig. 5.

The current-sensing power MOSFET is a five-terminal device. Switches S_1 and S_2 have identical unit cell structures and reside on the same silicon substrate. Their gate terminals are connected to a common terminal G, and their drain terminals are connected to a common terminal D. The source terminals of switch S_2 are connected to a current sense or mirror terminal S, and the source terminals of switch S_1 are connected to a main terminal M, which consists of Kelvin-sense terminal K and source terminal S. A Kelvin-sense terminal is internally shorted to the source terminal of switch S_1 to bypass the packaging and interconnection parasitic resistance associated with switch S_1, which provides more accurate current sensing.

The most common practice of using S_1 and S_2 for current sensing in a buck converter is shown in Fig. 6. N is the predetermined ratio of the transistor cells of switch S_1 to switch S_2. For example, N may be on the order of 100–1000. If N increases, the accuracy of the circuit decreases. All the transistor cells of the current-sensing power MOSFET are similar; therefore,

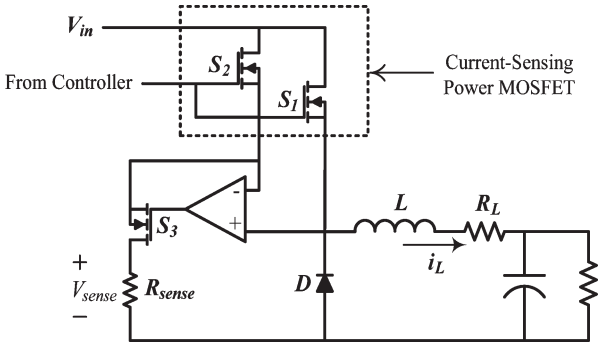

Fig. 6. Current-sensing power MOSFET-based current sensing.

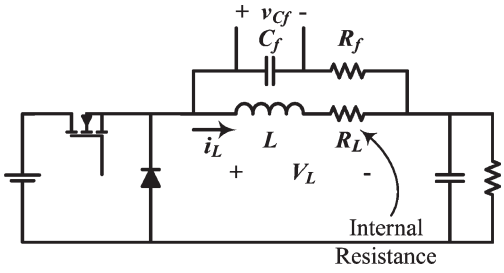

Fig. 7. Filter-based current-sensing technique.

if the sources of switches S_1 and S_2 are virtually connected, switches S_1 and S_2 pass currents in the ratio of $N:1$ and have resistances in a $1:N$ ratio.

An operational amplifier in Fig. 6 is used to make the gate-to-source voltages of both switches virtually equal. Since only a predetermined fraction of the total current is passing through R_{sense}, power dissipation in R_{sense} is low. Considering a typical range for the duty ratio when it is not too close to 0.0%, sense voltage V_{sense} in this technique is given by

$$V_{\text{sense}} = R_{\text{sense}} \left(\frac{i_L}{N} \right). \tag{8}$$

The utilization of current-sensing power MOSFET is impeded by its limited availability and high cost. This method is not applicable to high-frequency systems, because it introduces switching transients and noise to the sense signal. The accuracy of this method is limited, because it works only when switches S_1 and S_2 are matched. Since this technique's current ratio is $N:1$, a low degree of coupling between S_1 and S_2 can induce a significant error, and consequently, large spikes are injected in the sense signal during high-di/dt periods.

F. Filter-Based Current Sensing

Earlier, in Section II-B, it was described how the internal resistance of an inductor could be used to measure its current. In the section, an identical coupled inductor was used. A more applicable approach is to employ a passive *RC* filter, instead of a coupled inductor, as shown in Fig. 7. The voltage across filter capacitor C_f can be described as

$$V_{Cf}(s) = \left(\frac{R_L + Ls}{1 + R_f C_f s} \right) i_L(s). \tag{9}$$

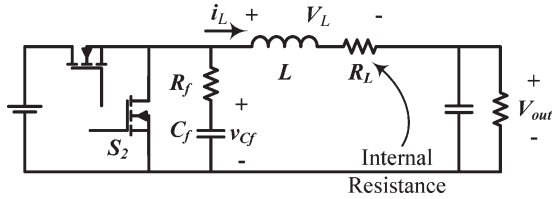

Fig. 8. Filter-based average current sensing.

The parallel $R_f C_f$ filter is designed in such a way that the following holds:

$$R_f C_f = \frac{L}{R_L}. \tag{10}$$

In that case, one can describe inductor current $i_L(t)$ as

$$i_L(t) = \frac{v_{Cf}(t)}{R_L}. \tag{11}$$

This technique is popular due to its accuracy, losslessness, low noise sensitivity, and high bandwidth. Other advantages include continuous current measurement, low cost, and PCB space saving [75]. The sensitivity of this method to temperature, switching frequency, and inductor current is analyzed in [21]. Yan *et al.* [8] have successfully applied this method to a power electronic converter with coupled inductors. The effect of time-constant mismatches on the performance of the sensing network is analyzed in [76]. In [76] and [77], the addition of a negative temperature coefficient resistive network is proposed to compensate for the temperature variations of R_L. Furthermore, to overcome the time-constant mismatching issue, a modified digital autotuning approach is presented in [24]. A mismatch of time constants [see (10)] causes load transients, which create a large change in the value of voltage V_{Cf}. This change is sensed by a load transient detector. The controller measures the derivative of the V_{Cf} signal and adjusts the value of variable resistor R_f to compensate for the time-constant mismatch. To satisfy (10), a self-learning scheme is proposed in [27]. In the proposed method, during the power converter start-up process, the parameters of the filter are self-tuned and self-calibrated.

G. Filter-Based Average Current Sensing

The filter-based current measurement technique can also be applied to applications in which only the average value of the inductor current needs to be measured. For instance, in average current-mode control, there is no need to find the instantaneous value of the current. The circuit diagram of a filter-based average current-sensing network is shown in Fig. 8 [6], [28]. The $R_f C_f$ filter is connected across the low-side switch S_2 of a synchronous buck converter.

Inductor voltage V_L contains ac and dc components. In the steady-state operation, the average value of its ac components is zero. This technique measures the average dc voltage across the inductor, which is only a dc voltage across internal resistor R_L. Therefore, by measuring the average inductor voltage, it is possible to measure average inductor current $\langle i_L \rangle$. The value of R_f must be selected to be much greater than the internal

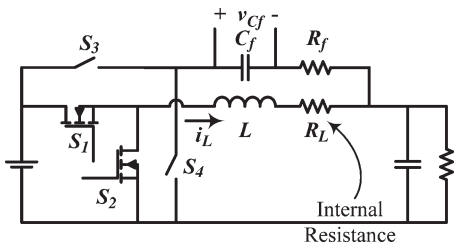

Fig. 9. Combined filter-based current-sensing technique.

resistance of the switches. Another requirement is to make sure that

$$R_f C_f \gg \text{switching frequency}. \tag{12}$$

Under steady-state conditions, the average value of the current passing through C_f is zero. Therefore, there is no average voltage drop across resistor R_f. As a result, the voltage across capacitor C_f will be equal to

$$\langle V_{Cf} \rangle = V_{\text{out}} + \langle i_L(t) \rangle R_L \tag{13}$$

or

$$\langle i_L(t) \rangle = \frac{\langle V_{Cf} \rangle - V_{\text{out}}}{R_L}. \tag{14}$$

From (14), it is inferred that the average inductor current is only affected by R_L. The values of R_f, C_f, L, and the switch resistances have no effect on the current-sensing result. This technique has successfully been used in interleaved parallel dc–dc converters to balance the average load currents in various channels [28]. This technique is useful for low-frequency measurements only. Its main drawback is that, for an accurate current sensing, the value of R_L must be known. This technique provides information about the average current only; it gives no information about the ac and transient current values.

H. Combined Filter-Based Current Sensing

The internal resistance of an inductor is usually relatively small. As a result, in the filter-based current-sensing method, measured voltage $v_{cf}(t)$ has a small magnitude and, therefore, is very sensitive to noise. At the same time, it is not efficient to place an external resistance in series with the inductor to boost up the magnitude of the measured voltage level. To overcome this problem, Chang [25] and Lethellier [26] have proposed a combined filter-based current-sensing method in which the internal resistance of switches (in this case, power MOSFETs) will be placed in series with the internal resistance of the inductor to build up a larger resistor. As shown in Fig. 9, the combined sense technique includes additional switches S_3 and S_4, which have gate signals that are identical with those of S_1 and S_2, respectively. The sensing network is configured so that, in any switching state, the internal resistance of a power MOSFET (R_{DS}) is placed in series with R_L. The increased sense circuit resistance increases the amplitude of voltage $v_{cf}(t)$; therefore, the output signal is clean and less susceptible to noise. It is worth mentioning that the new equation to be satisfied is $R_f C_f = L/(R_L + R_{DS})$.

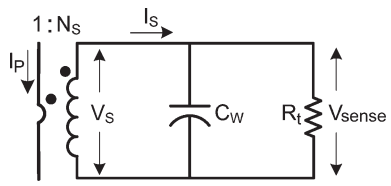

Fig. 10. Basic circuit of a single-turn primary CT.

III. Electromagnetic-Based Current-Sensing Techniques

A. Using a Current Transformer

A CT is similar to a voltage transformer, except that the primary input is a current. The four basic types of CTs [78], [79] include ac CTs (ACCTs), unidirectional CTs (UCTs), dc CTs (DCCTs), and flyback-type CTs (FBCTs). ACCTs and UCTs are commonly used; DCCTs are used for high-current applications, and FBCTs are used when current pulses are very short.

For typical switching converter applications, a CT has a single-turn primary and a multiturn secondary. The basic CT schematic is shown in Fig. 10. The primary is formed by wire from which an unknown current is passing. The secondary has a large number of turns, and it is terminated by terminating or burden resistor R_t. If the number of the secondary turns is too large, then there will be a significant interwinding capacitance C_W. In addition to primary and secondary windings, capacitance C_W is also added in the model of a CT. One of the most commonly used CTs is known as the clamp-on or clip-on type. It has a laminated core, which is arranged in such a manner that it can be opened by pressing a switch permitting the admission of the current-carrying conductor. The current-carrying conductor acts as a single-turn primary, whereas the secondary is connected across the standard ammeter.

The relationship between currents I_P and I_S, in this case, is given by

$$\frac{I_S}{I_P} = \frac{1}{N_S}. \tag{15}$$

Capacitor C_W is not considered here since the measured frequency is low. The secondary output voltage V_{sense} in a CT is proportional to resistor R_t based on the current flowing through it. Voltage V_{sense} across the secondary is given by

$$V_{\text{sense}} = I_S R_t = \frac{I_P}{N_S} R_t. \tag{16}$$

The CTs can only measure ac currents. However, it is possible to measure the current flowing through the switching components of a converter. This is based on the fact that the value of the current is zero when the switching device is off. The secondary voltage of the CT can be sampled and held during the off time of the switch and then subtracted from the secondary voltage waveform of the CT (see Fig. 11). Mammano [65] managed to measure the currents of both switches in a buck

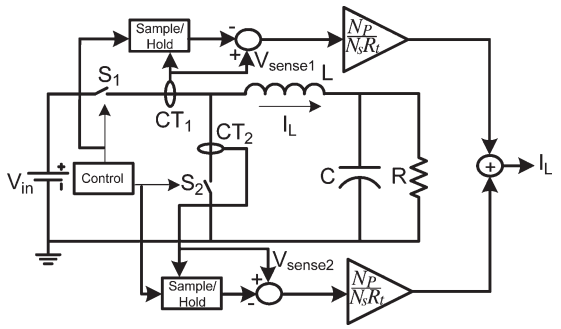

Fig. 11. Inductor current reconstruction using two ACCTs.

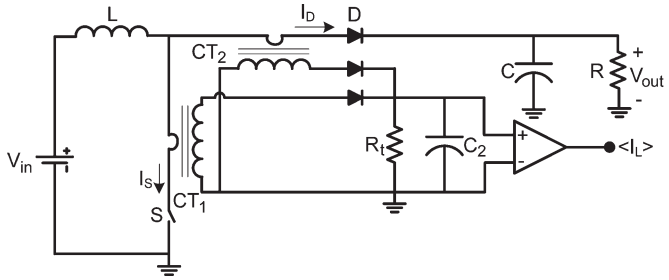

Fig. 12. Average inductor current sensing using two CTs.

converter and then reconstruct the inductor current waveform by adding them. In addition, several approaches using ACCTs and UCTs in power electronics applications are reported in [31]–[38].

B. Using a Current Transformer to Measure the Average Value of a Current

Transformers are used to measure the "switched" current and not the "average" current delivered to the load. However, in this section, different current-sensing techniques using CTs for average inductor current measurement are described [39]. In a boost converter, two CTs are used to sense the switch and diode currents and consequently measure the average inductor current, as shown in Fig. 12. CT_1 measures switch current I_S, and CT_2 measures diode current I_D. The outputs of the two CTs are then added to get the average value of the inductor current. The output is accurate in both the waveform and dc value. As the two transformers may not exactly have the same number of turns, this method may not be able to provide very accurate information about the average current.

Another technique for measuring the average inductor current in a forward converter is shown in Fig. 13. This method, which uses only one CT, replicates the inductor current waveform that appears as capacitor voltage V_{C2}. Voltage V_{C2} accurately follows the ac and dc excursions of the inductor current. When switch S is on, the CT measures the inductor current. The output of CT is converted into a voltage signal using resistor R_1. This voltage is then used to charge capacitor C_2, which gives the rising portion of the inductor current. When switch S is off, the CT gets reset, and capacitor C_2 is discharged through resistor R_2, which gives the downslope of the inductor current. The downslope of the inductor current can also be measured by using the circuit shown in Fig. 14. The second winding generates the discharge current for capacitor C_2 through current mirroring. By using the main inductor as a CT, isolation is achieved with both charge and discharge signals. In all of the previously discussed techniques in this section, the sensing circuits have their own grounds. Therefore, the sensing circuit can reside on either side of the isolation boundary.

C. Using an Air Core

The performance of a CT is often limited by the characteristics of its magnetic core material [hysteresis, nonlinearity, losses, saturation, and remanence (residual flux)]; therefore, the design of an air core or coreless transformer is often considered. The challenge with air core current-measurement techniques is to have enough measurement sensitivity and to be insensitive to external magnetic fields.

The Rogowski coil is a simple, inexpensive, and accurate approach for current measurement. The structure of a Rogowski coil is similar to that of a CT. However, instead of an iron core, the Rogowski coil is based on air or ironless bobbins with hundreds or thousands of turns, as shown in Fig. 15. The Rogowski coil has an air core, and therefore, it will never get saturated; therefore, its output will remain linear for high-current measurement [29], [40]–[42]. The conductor from which the unknown current flows is surrounded by the Rogowski coil for current measurement, as shown in Fig. 15. To place the current-carrying conductor inside the Rogowski coil, it can be opened without interrupting the circuit. The magnetic field produced by the current induces a voltage in the secondary coil, i.e., E.

Voltage E is proportional to the time derivative of the current flowing through the conductor, which is given by

$$E = M * \frac{dI_P}{dt}. \tag{17}$$

Here, I_P is the unknown primary current, and M is the mutual inductance of the circuit. M depends on the geometric parameters of the coil and is given by

$$M = \frac{\mu_o A N_S}{l} \tag{18}$$

where μ_0 is the permeability of free space, A is the cross-sectional area of the coil, N_S is the total number of secondary winding turns, and l is the mean path length of the coil. Since the derivative of the direct current is zero, the Rogowski coil current sensor cannot measure dc currents. It is used to measure ac and pulsed dc currents only.

The phase-delayed secondary voltage is integrated to produce an output voltage V_{sense} that is proportional to current I_P. If the Rogowski coil is used to measure the current in a semiconductor switch, a simple resistor–capacitor integrator, as shown in Fig. 15, can be used to reproduce the current waveform as voltage. The Rogowski coil terminals are connected in a special way to avoid the external field effects. The output voltage of the integrator circuit is given by

$$V_{\text{sense}} = \frac{1}{RC}\int E * dt = \frac{1}{RC}\frac{\mu_0 A N_S}{l} I_P \tag{19}$$

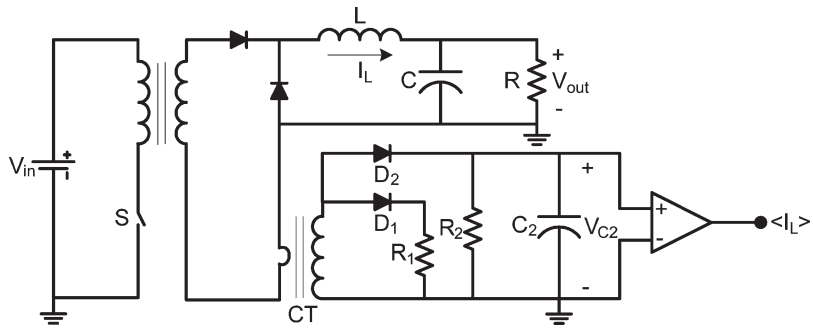

Fig. 13. Average inductor current sensing using one CT.

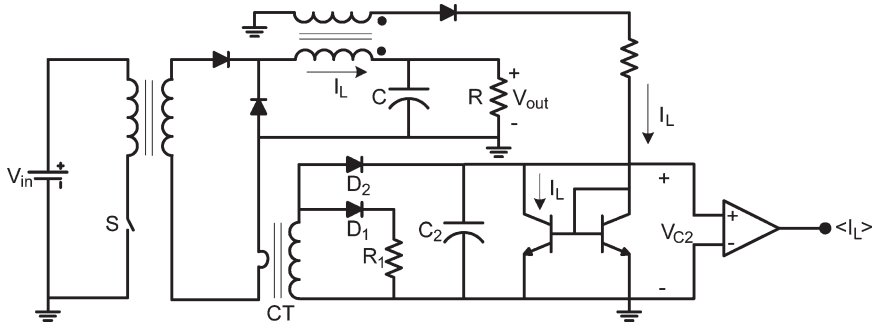

Fig. 14. Average inductor current sensing by adding second winding on the existing inductor.

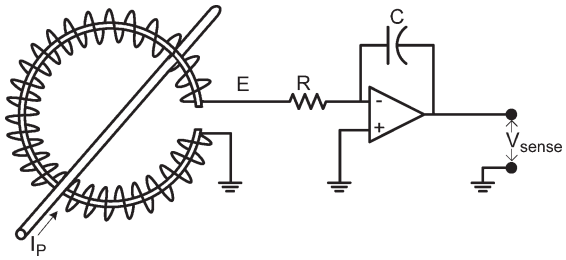

Fig. 15. Rogowski coil current sensor.

which is proportional to unknown current I_P.

The Rogowski coil works with a wound coil. The mechanically open structure of the Rogowski coil can create a slight gap in the coil structure, which leads to errors (below 1% with a maximum of 2%) based on the position of the current-carrying conductor in the aperture. This method's accuracy is affected by the external field due to the manufacturing tolerance of the wound coil. A planar Rogowski coil current sensor is the solution to these problems [43].

D. Using Fiber Optics

An FOCS determines the current flow in an electrical conductor by measuring the magnetic field density within the vicinity of the conductor [57]–[61]. The operation principal is based on the Faraday effect. When a polarized monochromatic light propagates in parallel to a magnetic field, the polarization direction rotates, as shown in Fig. 16.

The polarization angle is proportional to the magnetic field circulation on the optical path. The angular rotation experienced by the light passing through the sensor is given by

$$\theta = VBl \tag{20}$$

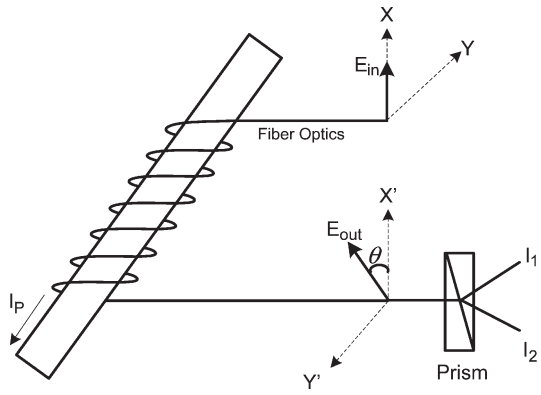

Fig. 16. Polarimetric FOCS.

where V is the Verdet constant of the material used for the sensor, B is the magnetic flux density, and l is the length of the FOCS exposed to the magnetic field. The polarization angle also depends on the light wavelength and fiber material. The FOCS measures the exact integral of the magnetic field along the closed-loop created by the fiber. A true current reading is obtained if the FOCS completely encloses the conductor; otherwise, the reading reflects the magnetic field intensity at the measurement point and has to be scaled accordingly.

FOCSs are classified as intrinsic and extrinsic types. An intrinsic sensor uses fiber for current sensing, whereas an extrinsic sensor uses bulk optic. On the other hand, there are three different approaches of FOCS, i.e., bulk, polarimetric, and interferometric. Bulk current sensors have high-Verdet-constant crystals, resulting in excellent sensitivity. Optical fibers have a lower Verdet constant, but many turns of the fiber around the conductor result in improved sensitivity. The polarimetric

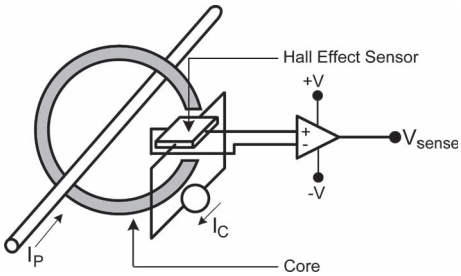

Fig. 17. Open-loop Hall-effect current sensor with a single-turn primary.

sensor measures the rotation of a linear polarization, whereas the interferometric sensor using a Sagnac interferometer measures the nonreciprocal phase shift.

E. Using Hall Effect

Hall-effect sensors are used to measure ac and dc currents with electrical isolation. It is used to measure the current without interrupting the circuit. A Hall-effect sensor is small, provides noise-immune signal, and consumes little power [44]–[48]. A Hall-effect sensor works based on the Lorentz force, which acts on charges moving through a magnetic field. The Hall-effect principle states that, when a magnetic field is applied to a conducting or semiconducting material through which a current is flowing, a voltage will be developed across the sides of the material.

If I_C is the control current passing through the Hall sensor, B is the magnetic flux density created by the unknown current-carrying conductor, K is a constant of conducting material, d is the thickness of the sheet, and $V_{\rm OH}$ is the offset of the Hall sensor in the absence of the external field, the output Hall voltage V_H of a Hall-effect sensor is given by

$$V_H = \frac{K}{d} B I_C + V_{\rm OH}. \tag{21}$$

Flux density B for a Hall-effect sensor is inversely proportional to the distance from the center of the conductor to the point of sensing; therefore, usable flux density cannot be achieved at a much greater distance from the conductor's center. Other disadvantages of Hall-effect sensors include low sensitivity, the need for a concentrator, tricky mechanical positioning, limited linearity range, sensitivity to mechanical stresses and ambient temperature variations, limited maximum frequency range due to junction capacitance, and the requirement for an isolated power supply. Different Hall-effect-based current measurement techniques have been proposed to overcome the aforementioned disadvantages. These techniques include open-loop Hall-effect sensing, closed-loop Hall-effect sensing, and combinations of open- and closed-loop Hall-effect sensing with a CT technique.

An open-loop Hall-effect current sensor uses a high-permeability magnetic core (as a field concentrator) with an air gap located around the conductor, which carries current I_P, as shown in Fig. 17 [49]–[51]. A linear Hall sensor is inserted into the air gap and provides voltage V_H proportional to flux density B produced by current I_P. Voltage V_H is amplified, and the output voltage is then read as a voltage that represents current I_P through a scaling factor.

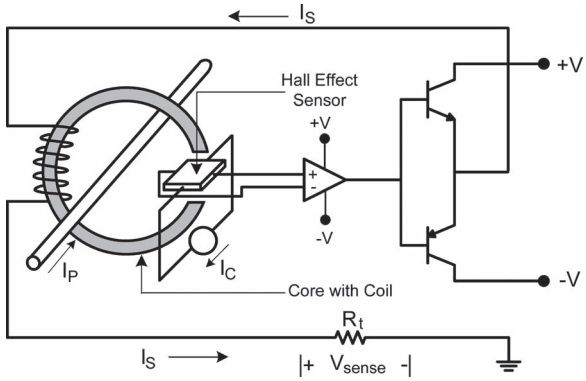

Fig. 18. Closed-loop Hall-effect current sensor.

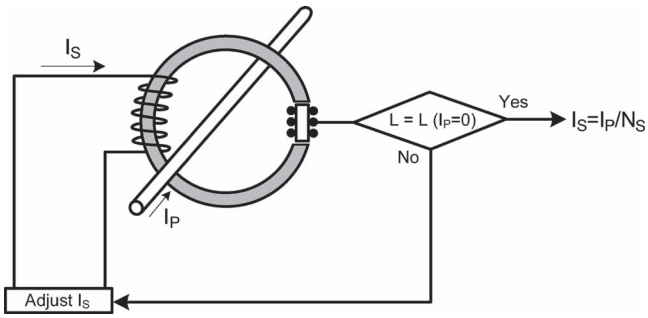

Fig. 19. Saturable inductor current sensor.

Open-loop Hall-effect current sensors are able to accurately measure ac, dc, and complex currents. The benefits of an open-loop Hall-effect current sensor include simple construction, low cost, low power consumption, low insertion losses, and small size for higher currents. However, the disadvantages include magnetic core heating due to core losses at high-frequency current measurements, a narrow bandwidth (dc to 25 kHz), a high offset and gain drift, a limited range of linearity, and lower accuracy.

A closed-loop Hall-effect current sensor improves the performance of an open-loop Hall-effect current sensor by using a compensation circuit, as shown in Fig. 18. In a closed-loop Hall-effect sensor, a low-current secondary winding is wrapped around the high-permeability core to develop magnetic flux in opposition to the flux developed by current I_P [52]–[54]. The Hall sensor is enclosed in an overall feedback loop, as shown in Fig. 18. The Hall sensor in the air gap produces voltage V_H proportional to the flux density in the core. Voltage V_H is then amplified by the operational amplifier and fed into a push–pull amplifier. Compensation current I_S is fed by the push–pull amplifier into the secondary coil to null the flux in the core. The Hall sensor in the air gap is also used to detect zero flux. Therefore, the closed-loop Hall-effect sensors are also known as compensated or zero-flux Hall-effect current sensors. Current I_S creates flux equal in amplitude—but opposite in direction—to the flux created by current I_P. Operating the core near zero flux eliminates the dependence on the linearity of the core and Hall sensor and reduces hysteresis errors.

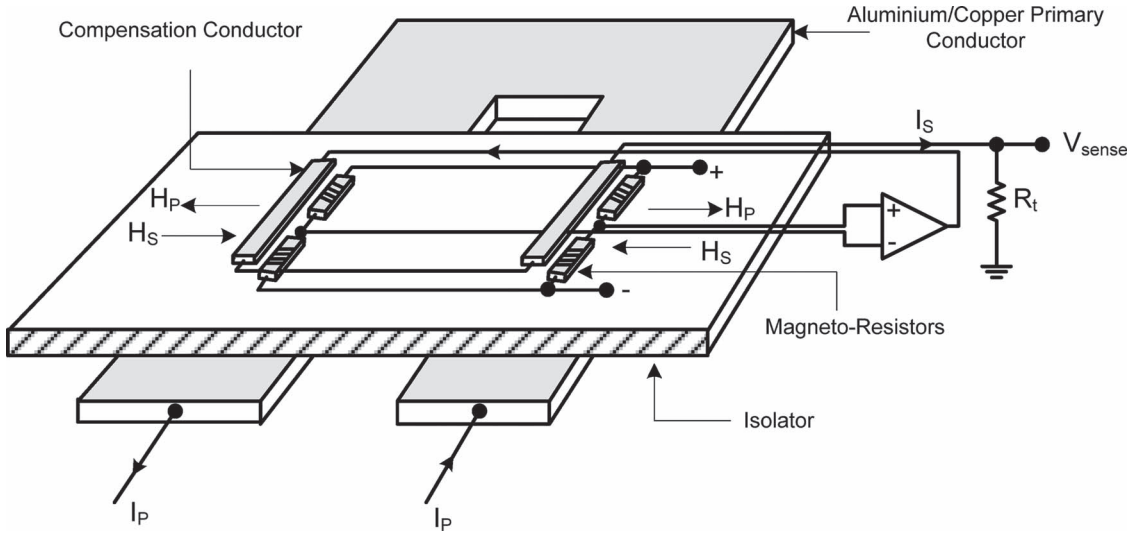

Fig. 20. Barberpole MR sensor with compensation circuit.

When the magnetic flux is fully compensated, the ampere turns of the two windings are identical, which is given by

$$N_P I_P = N_S I_S. \tag{22}$$

Closed-loop Hall-effect current sensors are able to accurately measure ac, dc, and complex currents. Closed-loop Hall-effect current sensors provide many advantages, such as high bandwidth (dc to 200 kHz), high accuracy and linearity, fast response time, low insertion losses, and low gain drift. However, their disadvantages include higher cost, high current consumption, larger dimensions, and limited output current due to the fact that closed-loop sensors can only drive a finite amount of secondary current. It is also possible to combine an open-loop Hall-effect sensing or a closed-loop Hall-effect current sensor with a CT. More information about this technique is given in [55] and [56].

F. Using a Saturable Inductor

Saturable inductor current sensors work on the same measurement principle as Hall-effect-based current sensors. The magnetic field created by the primary current to be measured is detected by a specific sensing element [62]. The design of the saturable inductor current sensor is similar to that of a closed-loop Hall-effect current sensor; the only difference is that this method uses a saturable inductor, instead of a Hall-effect sensor, in the air gap. A saturable inductor current sensor is based on the detection of an inductance change, as shown in Fig. 19.

The saturable inductor is made of a small and thin magnetic core wound with a coil around it. The saturable inductor operates in its saturation region. It is designed in such a way that the external and internal flux densities will affect its saturation level. Changes in the saturation level of a saturable inductor will alter its permeability and, consequently, its inductance L. The value of saturable inductance L is high at low currents (based on the permeability of the core) and low at high currents (the core permeability becomes unity when saturated).

Fig. 19 shows a saturable inductor current sensor using one core. High-frequency performance is achieved by using two cores without air gaps. One of the two main cores is used to create a saturable inductor, and the other is used to create a high-frequency transformer effect. In another approach, three cores can be used without an air gap. Two of the three cores are used to create a saturable inductor, and the third core is used to create a high-frequency transformer effect. More information about these techniques is given in [62].

It is difficult to compare different saturable inductor techniques. The advantages of saturable inductor sensors include high resolution, high accuracy, low offset and gain drift, and large bandwidth (up to 500 kHz). The drawbacks of saturable inductor technologies include the limited bandwidth for simpler design, relatively high secondary power consumption, and risk of current or voltage noise injection into the primary conductor.

G. Using a Magnetoresistor

Every conducting material has some magnetoresistance. This magnetoresistance effect is large in Permalloys (Fe-Ni) and other ferromagnetic materials. An MR is a two-terminal device that parabolically changes its resistance with the applied magnetic field. This variation of the resistance of MR due to the magnetic field is known as the anisotropic magnetoresistive effect. More information about this technique is given in [63] and [64]. An MR sensor with a compensation circuit is shown in Fig. 20.

An MR device cannot detect the direction of field H_y and has vanishing sensitivity for low fields. The nonlinearity and nondirectionality of an MR device are corrected by modifying the MR transfer curve using a barberpole configuration [63]. External magnetic fields can distort the current measurement of a barberpole MR sensor. To avoid this distortion, barberpole MR devices can be configured into Wheatstone bridge configuration (see Fig. 20).

Even with the barberpoles, the linearity of the MR device is not very high; therefore, a compensation circuit is required,

TABLE I
COMPARATIVE OVERVIEW OF DIFFERENT RESISTIVE- AND ELECTROMAGNETIC-BASED CURRENT-SENSING TECHNIQUES

Techniques	Advantages	Disadvantages
Using an externally added resistor	Simple, accurate, low cost	Power loss incurred by sense resistor
Using the internal resistance of an inductor	Accurate, lossless	Not useful for high power applications
MOS current sensing	Lossless, accurate	Complicated circuit, accuracy depends on the matching performance of the current mirror
Using the internal resistance of a MOSFET	Lossless, no additional sensing component required, low cost	Not accurate for high input voltages and high switching frequencies, affected by the temperature variations of R_{DS}, discontinuous, and noisy
Using MOSFET R_{DS}-based current sensing with self-calibration	Lossless, accurate, combination with lossless techniques is also possible	Addition of an extra circuit, limited applications
Using current-sensing power MOSFET	Lossless, practical, accurate with respect to temperature variations, no additional sensing component required, low cost	Special MOSFET, introduce switching transients and noise at high frequencies, accuracy depends on the matching performance of the current mirror, switching noise, limited applications, discontinuous and noisy
Using filter-based current sensing	Lossless, continuous current measurement, low cost, low switching noise, high power efficiency	Low accuracy due to unknown L and R_L, filter design, temperature dependence, tolerance of components, time constant mismatching, only for off-chip applications, changes in the inductance due to a dc current bias
Using filter-based current sensing with self-tuning	Lossless, accurate, matched time constants, continuous current measurement	Complicated circuit, filter design
Using combined-sense technique	Lossless, accurate, continuous current measurement, low cost, improved SNR	Complicated circuit, filter design, unmatched R_{DS} of main MOSFET switches, time constant mismatching
Using filter-based current sensing with self-tuning and self-calibration	Lossless, accurate, low switching noise, matched time constants, continuous current measurement, fully integrated	Complicated circuit, separate filter design for each application, accuracy of this technique depends on the tuning and calibration accuracy
Using a filter	Lossless, easily integrated on IC chip	Unknown R_L, information of average inductor current only, sensing dependence on Rf and Cf
Using two CTs	Simple, lossless	Requirement of two matched sensing transformers
Using one CT	Simple, lossless	Not very accurate, limited applications
Using inductor as a sense transformer	Simple, accurate, lossless	Additional winding, requirement of a high voltage isolation for off line converters
Using ACCT	Lossless, good SNR, good common mode rejection	Measures only ac currents, core limitations, limited frequency range, not suitable for multiple-inductor converters
Using ACCT with sample-and-hold	Accurate, low power loss, able to measure ac current having dc current component	Requires high bandwidth sample-and-hold ICs and two transformers, core limitations
Using UCT	Lossless, accurately measures ac current having dc current component	Not suitable for higher switching frequencies, core limitations
Using Rogowski Coil	Accurate, low weight, no dc current saturation, low sensitivity to parameter variations, ac and pulsed dc current measurements	External circuit is required to analyze the output, open structure leads to measurement error, error is introduced by processing electronics
Using planar Rogowski Coil	Lossless, ac and pulsed dc current measurements accurate, light and small, insensitive to external field perturbations and conductor position inside the coil	Expensive, external circuit is required to analyze output, complicated circuit, high secondary power consumption
Using FOCS	Lossless, no electromagnetic interference, small sensing elements, ac and dc current measurement	Expensive, environmental sensitivity
Using open-loop Hall-effect current sensor	Low secondary power consumption, small size, low cost, ac, dc, and complex current measurements	Low sensitivity, temperature dependent output, linearity errors, prone to static drift, core limitations
Using closed-loop Hall-effect current sensor	Accurate, ac, dc, and complex current measurements, fast response time, wide bandwidth, low temperature drift	Compensation circuit is required, high secondary current consumption, expensive, bulky for low currents, core limitations
Using saturable inductor current sensor with one core	High resolution, high accuracy, ac and dc current measurement	Limited bandwidth, high secondary power consumption, core limitations
Using MR current sensor	Smaller volume and weight, no remanence, ac and dc current measurement, high sensitivity, noise immunity	Placement of barberpoles in the Wheatstone bridge configuration, limited frequency response due to the magnetic inertia of permalloy and skin effect of the current carrying conductor

as in the closed-loop Hall-effect current sensor. An electrically isolated aluminum compensation conductor is integrated on the same substrate above the Permalloy resistors, as shown in Fig. 20. The output of the Wheatstone bridge is connected to the input of an operational amplifier, which generates the compensating current I_S. Current I_S then flows through the aluminum conductor to generate a magnetic field that exactly compensates the field created by current I_P. The bridge output voltage is usually close to zero; therefore, sensor nonlinearity is minimized. Current I_S is then measured through resistor R_t, which is an exact representation of current I_P. To have the same amplitude but opposite directions of the magnetic fields on two arms of the bridge, the primary current conductor under the substrate is U shaped.

IV. COMPARATIVE OVERVIEW

Table I summarizes the advantages and disadvantages of different resistive- and electromagnetic-based current-sensing techniques.

V. Conclusion

For safety, improved performance, and feedback control of switched-mode power converters and motors, it is often necessary for the controller to better understand its operating environment, particularly the input and/or output currents. In addition, current sensing is the most common method for the battery state of charge estimation. The most common current-sensing method is to insert a resistor in the path of an unknown current. This method incurs significant power losses for high currents. In this paper, different alternatives for accurate and lossless current measurements have been presented, and the advantages and disadvantages of each technique have been discussed. For accurate and continuous current measurement, different current-sensing options with self-tuning and/or self-calibration have been evaluated. Many applications require the average current information for control purposes. Several average current-sensing methods have been reviewed in this paper. Different electromagnetic-based current-sensing techniques, which are used to achieve high-bandwidth current measurements, have also been analyzed in this paper.

References

[1] S. Wall, "Vector control: A practical approach to electric vehicles," in *Proc. IEEE Colloq. Vector Control Direct Torque Control Induction Motors*, 1995, pp. 5/1–5/7.

[2] T. Wang, X. Zhou, and F. Lee, "A low voltage high efficiency and high power density dc–dc converter," in *Proc. IEEE Power Electron. Spec. Conf.*, 1997, pp. 240–245.

[3] W. Kester and B. Erisman, "Switching regulators," *Analog Devices Technical Library on Power Management*, 1999.

[4] L. Peng and B. Lehman, "A design method for paralleling current mode controlled DC–DC converters," *IEEE Trans. Power Electron.*, vol. 19, no. 3, pp. 748–756, May 2004.

[5] Y. Chi, P. Mok, N. Ka, and M. Chan, "An integrated CMOS current-sensing circuit for low-voltage current-mode buck regulator," *IEEE Trans. Circuits Syst. II, Exp. Briefs*, vol. 52, no. 7, pp. 394–397, Jul. 2005.

[6] Z. Xunwei, P. Xu, and F. C. Lee, "A high power density, high efficiency and fast transient voltage regulator module with a novel current sensing and current sharing technique," in *Proc. IEEE Appl. Power Electron. Conf. Expo.*, Mar. 14–18, 1999, pp. 289–294.

[7] L. H. Dixon, "Average current mode control of switching power supplies," in *Proc. Unitrode Power Supply Des. Semin.*, 1988, pp. 5.1–5.14.

[8] D. Yan, X. Ming, and F. Lee, "DCR current sensing method for achieving adaptive voltage positioning (AVP) in voltage regulators with coupled inductors," in *IEEE Power Electron. Spec. Conf.*, Jun. 2006, pp. 1–7.

[9] Z. Bin, A. Huang, Z. Xigen, L. Yunfeng, and S. Atcitty, "The built-in current sensor and over-current protection of the emitter turn-off (ETO) thyristor," in *Conf. Rec. IEEE IAS Annu. Meeting*, Oct. 2003, pp. 1264–1269.

[10] M. Margala and I. Pecuh, "Testing of deep-submicron battery-operated circuits using new fast current monitoring scheme," in *Proc. IEEE Int. Workshop Defect Based Testing*, Apr. 30, 2000, pp. 65–69.

[11] O. Barbarisi, R. Canaletti, L. Glielmo, M. Gosso, and F. Vasca, "State of charge estimator for NiMH batteries," in *Proc. IEEE Conf. Decision Control*, Dec. 2002, pp. 1739–1744.

[12] J. Sun, J. Zhou, M. Xu, and F. Lee, "A novel input-side current sensing method to achieve AVP for future VRs," *IEEE Trans. Power Electron.*, vol. 21, no. 5, pp. 1235–1242, Sep. 2006.

[13] R. Lenk, "Application bulletin AB-20 optimum current sensing techniques in CPU converters," in *Fairchild Semiconductor Application Notes*. South Portland, ME: Fairchild Semicond. Corp., 1999.

[14] H. P. Forghani-zadeh and G. Rincon-Mora, "Current-sensing techniques for DC–DC converters," in *Proc. 45th Midwest Symp. Circuits Syst.*, Aug. 2002, pp. II-577–II-580.

[15] *High-Side Current-Sense Measurement: Circuits and Principles*. App. Note 746-MAX4080.

[16] *Zetex AN39-Current Measurement Applications Handbook*, Zetex Semiconductors, Dallas, TX, no. 5, Jan. 2008.

[17] W. Ki, "Current sensing technique using MOS transistor scaling with matched current sources," U.S. Patent 5 757 174, May 26, 1998.

[18] G. Rincon-Mora and P. Forghani, "Accurate and lossless current-sensing techniques: A practical myth?" *Power Management Design Line*, Mar. 17, 2005.

[19] "Three phase buck PWM controller with two integrated MOSFET drivers and one external driver signal," *INT6566A Data Sheet*, Jul. 27, 2005, Milpitas, CA: Intersil.

[20] H. P. Forghani-zadeh and G. Rincon-Mora, "A lossless, accurate, self-calibrating current-sensing technique for DC–DC converters," in *Proc. IEEE Ind. Electron. Soc. Annu. Conf.*, Nov. 6–10, 2005, pp. 549–554.

[21] E. Dallago, M. Passoni, and G. Sassone, "Lossless current sensing in low-voltage high-current DC/DC modular supplies," *IEEE Trans. Ind. Electron.*, vol. 47, no. 6, pp. 1249–1252, Dec. 2006.

[22] Z. Yang, R. Zane, A. Prodic, R. Erickson, and D. Maksimovic, "Online calibration of MOSFET on-state resistance for precise current sensing," *IEEE Power Electron. Lett.*, vol. 2, no. 3, pp. 100–103, Sep. 2004.

[23] Z. Yang, R. Zane, A. Prodic, R. Erickson, and D. Maksimovic, "On-line calibration of lossless current sensing," in *Proc. IEEE Appl. Power Electron. Conf. Expo.*, 2004, pp. 1345–1350.

[24] G. Garcea, S. Saggini, D. Zambotti, and M. Ghioni, "Digital auto-tuning system for inductor current sensing in VRM applications," in *Proc. IEEE Appl. Power Electron. Conf. Expo.*, Mar. 2006, pp. 493–498.

[25] C. Chang, "Combined lossless current sensing for current mode control," in *Proc. IEEE Appl. Power Electron. Conf. Expo.*, 2004, pp. 404–410.

[26] P. Lethellier, "Method and apparatus for sensing output inductor current in a DC-to-DC power converter," U.S. Patent 6 441 597 B1, Aug. 27, 2002.

[27] H. P. Forghani-zadeh and G. A. Rincon-Mora, "An accurate, continuous, and lossless self-learning CMOS current-sensing scheme for inductor-based DC-DC converters," *IEEE J. Solid-State Circuits*, vol. 42, no. 3, pp. 665–679, Mar. 2007.

[28] X. Zhou, P. Xu, and F. C. Lee, "A novel current-sharing control technique for low-voltage high-current voltage regulator module applications," *IEEE Trans. Power Electron.*, vol. 15, no. 6, pp. 1153–1162, Nov. 2000.

[29] A. Radun, "An alternative low-cost current-sensing scheme for high-current power electronic circuits," *IEEE Trans. Ind. Electron.*, vol. 42, no. 1, pp. 78–84, Feb. 1995.

[30] H. Marecar and R. Oruganti, "Fast and accurate current sensing in a multiphase buck converter," in *Proc. IEEE Int. Conf. Power Electron. Drives Syst.*, Jan. 2006, pp. 166–171.

[31] L. Wong, Y. Lee, and D. Cheng, "Bi-directional pulse-current sensors for bi-directional PWM DC-DC converters," in *Proc. IEEE Power Electron. Spec. Conf.*, Jun. 2000, pp. 1043–1046.

[32] K. Ma and Y. Lee, "Technique for sensing inductor and DC output currents of PWM DC–DC converter," *IEEE Trans. Power Electron.*, vol. 9, no. 3, pp. 346–354, May 1994.

[33] K. Ma and Y. Lee, "Novel technique for sensing inductor and DC output currents of PWM DC–DC converter," in *Proc. IEEE Appl. Power Electron. Conf.*, Feb. 23–27, 1992, pp. 345–351.

[34] N. McNeill, N. Gupta, and W. Armstrong, "Active current transformer circuits for low distortion sensing in switched mode power converters," *IEEE Trans. Power Electron.*, vol. 19, no. 4, pp. 908–917, Jul. 2004.

[35] A. Peterchev and S. Sanders, "Load-line regulation with estimated load-current feedforward: Application to microprocessor voltage regulators," *IEEE Trans. Power Electron.*, vol. 21, no. 6, pp. 1704–1717, Nov. 2006.

[36] J. Petter, J. McCarthy, P. Pollak, and C. Smith, "Survey of DC current measurement techniques for high current precision power supplies," in *Proc. IEEE Nucl. Sci. Symp. Med. Imaging Conf.*, Nov. 1991, pp. 961–967.

[37] E. Laboure, F. Costa, and F. Forest, "Current measurement in static converters and realization of a high frequency passive current probe (50 A–300 MHz)," in *Proc. 5th Eur. Conf. Power Electron. Appl.*, Sep. 1993, pp. 478–483.

[38] H. Strom, *Magnetic Amplifiers*. Hoboken, NJ: Wiley, 1955, p. 79. 167, 407.

[39] J. O'Connor, "The UC3848 average current mode controller squeezes maximum performance from single switch converters," *Unitrode Application Note-135*.

[40] D. Ward and J. Exon, "Experience with using Rogowski coils for transient measurements," in *Proc. IEE Colloq. Pulsed Power Technol.*, Feb. 20, 1992, pp. 6/1–6/4.

[41] A. Luciano and M. Savastano, "Wide band transformer based on a split-conductor current sensor and a Rogowski coil for high current measurement," in *Proc. IEEE Instrum. Meas. Technol. Conf.*, Apr. 1995, pp. 454–458.

[42] X. Chucheng, Z. Lingyin, T. Asada, W. Odendaal, and J. van Wyk, "An overview of integratable current sensor technologies," in *Conf. Rec. IEEE IAS Annu. Meeting*, Oct. 2003, pp. 1251–1258.
[43] E. Favre and W. Teppan, "State of the art in current sensing technologies," in *Proc. Power Electron. Intell. Motion Conf.*, Nov. 2003, pp. 549–554.
[44] R. Dickinson and S. Milano, *Isolated Open Loop Current Sensing Using Hall Effect Technology in an Optimized Magnetic Circuit*. Worcester, MA: Allegro MicroSystems, Nov. 2002.
[45] J. Pankau, D. Leggate, D. Schlegel, R. Kerkman, and G. Skibiniski, "High-frequency modeling of current sensors," *IEEE Trans. Ind. Appl.*, vol. 35, no. 6, pp. 1374–1382, Nov./Dec. 1999.
[46] K. Corzine and D. Sudhoff, "A hybrid observer for high performance brushless DC motor drives," *IEEE Trans. Energy Convers.*, vol. 11, no. 2, pp. 318–323, Jun. 1996.
[47] T. Matsuo, V. Blasko, J. Moreira, and T. Lipo, "Field oriented control of induction machines employing rotor end ring current detection," *IEEE Trans. Power Electron.*, vol. 9, no. 6, pp. 638–645, Nov. 1994.
[48] C. Chunshan, J. Wang, G. Cao, and X. Zhao, "Design of a new current sensing device for joint torque force control of the precision assembly robot," in *Proc. 5th World Congr. Intell. Control Autom.*, Jun. 2004, pp. 4609–4613.
[49] *LEM Current Sensors*, 2007. [Online]. Available: www.lem.com
[50] *Hall Effect Current Sensors*, 2007. [Online]. Available: www.bbautomacao.com
[51] *Current Measurement*, 2007. [Online]. Available: www.sypris.com
[52] D. Leggate, J. Pankau, R. Kerkman, D. Schlegel, and G. Skibiniski, "Reflected waves and their associated current," *IEEE Trans. Ind. Appl.*, vol. 35, no. 6, pp. 1383–1392, Nov./Dec. 1999.
[53] "Technical information," *Closed Loop Transducers With Small Footprint up to 100 A Nominal*, LEM, Geneva, Switzerland, Feb. 2003.
[54] R. Major, "Current measurement with magnetic sensors," in *IEE Colloq. Magn. Mater. Sens. Actuators*, Oct. 11, 1994, pp. 5/1–5/3.
[55] L. Dalessandro, N. Karrer, and J. Kolar, "High-performance planar isolated current sensor for power electronics applications," *IEEE Trans. Power Electron.*, vol. 22, no. 5, pp. 1682–1692, Sep. 2007.
[56] L. Ghislanzoni and J. Carrasco, "A DC current transformer for large bandwidth and high common-mode rejection," *IEEE Trans. Ind. Electron.*, vol. 46, no. 3, pp. 631–636, Jun. 1999.
[57] P. Mihailovic, S. Petricevic, Z. Stojkovic, and J. Radunovic, "Development of a portable fiber-optic current sensor for power systems monitoring," *IEEE Trans. Instrum. Meas.*, vol. 53, no. 1, pp. 24–30, Feb. 2004.
[58] J. Blake, "Fiber optic current sensor calibration," in *Proc. IEEE/PES Transmiss. Distrib. Conf. Expo.*, Oct./Nov. 2001, pp. 127–130.
[59] J. Blake and A. Rose, "Fiber-optic current transducer optimized for power metering applications," in *Proc. IEEE PES Transmiss. Distrib. Conf. Expo.*, Sep. 2003, pp. 405–408.
[60] P. Niewczas, W. Madden, W. Michie, A. Cruden, and J. McDonald, "Magnetic crosstalk compensation for an optical current transducer," *IEEE Trans. Instrum. Meas.*, vol. 50, no. 5, pp. 1071–1075, Oct. 2001.
[61] E. Vaerewyck and E. Anderson, "Electric motor and transformer load sensing technique," U.S. Patent 4 428 017, Jan. 24, 1984.
[62] "Technical Information," *CTs ITB 300-S, IT 400-S and IT 700-S High Accuracy—High Technology—Simply the Perfect Choice*, LEM, Geneva, Switzerland, Dec. 2005.
[63] E. Olson and R. Lorenz, "Integrating giant magnetoresistive current and thermal sensors in power electronic modules," in *Proc. IEEE Appl. Power Electron. Conf. Expo.*, Feb. 2003, pp. 773–777.
[64] G. Laimer and J. W. Kolar, "Design and experimental analysis of a DC to 1 MHz closed loop magnetoresistive current sensor," in *Proc. IEEE Appl. Power Electron. Conf. Expo.*, Mar. 2005, vol. 2, pp. 1288–1292.
[65] B. Mammano, "Current-sensing solutions for power-supply designers," in *Unitrode Design Note*. Dallas, TX: Texas Instruments, 1997.
[66] Y. Xiao, J. Cao, J. Chen, and K. Spring, "Current sensing trench power MOSFET for automotive applications," in *Proc. IEEE Appl. Power Electron. Conf. Expo.*, Mar. 2005, vol. 2, pp. 766–770.
[67] A. Sedra, G. Roberts, and F. Gohh, "The current conveyor: History, progress and new results," *Proc. Inst. Elect. Eng.*, vol. 137, no. 2, pp. 78–87, Apr. 1990.
[68] D. Grant and R. Pearce, "Dynamic performance of current-sensing power MOSFETs," *Electron. Lett.*, vol. 24, no. 18, pp. 1129–1131, Sep. 1988.
[69] P. Givelin, M. Bafleur, E. Tournier, T. Laopoulos, and S. Siskos, "Application of a CMOS current mode approach to on-chip current sensing in smart power circuits," *Proc. Inst. Elect. Eng.—Circuits, Devices Syst.*, vol. 142, no. 6, pp. 357–363, Dec. 1995.
[70] S. Yuvarajan and L. Wang, "Performance analysis and signal processing in a current sensing power MOSFET (SENSEFET)," in *Conf. Rec. IEEE IAS Annu. Meeting*, Sep./Oct. 1991, pp. 1445–1450.
[71] S. Clemente, H. Ishii, and S. Young, *International Rectifier AN-959: An Introduction to the HEXSense Current-Sensing Device*.
[72] D. Grant and R. Williams, "Current sensing MOSFETs for protection and control," in *Proc. IEE Colloq. Meas. Tech. Power Electron.*, Oct. 1992, pp. 8/1–8/5.
[73] M. Laxarus, K. Rabah, and P. Ripley, "Stabilised high power MOSFET modules," *Proc. Inst. Elect. Eng.—Commun., Speech, Vis.*, vol. 135, no. 6, pp. 155–158, Dec. 1988.
[74] S. MacMinn, W. Rzesos, P. Szczesny, and T. Jahns, "Application of sensor integration techniques to switched reluctance motor drives," *IEEE Trans. Ind. Appl.*, vol. 28, no. 6, pp. 1339–1344, Nov./Dec. 1992.
[75] "A simple-current sense technique eliminating a sense resistor," *LinFinity Application Note AN-7*.
[76] L. Hua and S. Luo, "Design considerations of time constant mismatch problem for inductor DCR current sensing method," in *Proc. IEEE Appl. Power Electron. Conf. Expo.*, Mar. 2006, pp. 1368–1374.
[77] N. A. Ismail, "Two phase buck converter with integrated high current 5V to 12V drivers," *Intersil Application Note 1197.1*.
[78] K. Bilings, *Switch Mode Power Supply Handbook*. New York: McGraw-Hill, 1989, ch. 14, pp. 3.176–3.192.
[79] B. Theraja and A. Theraja, *A Textbook of Electrical Technology in SI Units*, vol. 2. New Delhi, India: S. Chand, 2006, ch. 32 and 33, pp. 1115–1242.

Asha Patel received the B.Eng. degree in electrical engineering from Sardar Vallabhbhai National Institute of Technology, Surat, India, in June 2002 and the M.Sc. degree in electrical engineering from the Missouri University of Science and Technology, Rolla, in December 2007.

From 2002 to 2004, she was a Lecturer with the Diploma Engineering College, South Gujarat University, India. From 2006 to 2007, she was a Research Assistant, conducting research on bidirectional and step-down switched-capacitor converters under Dr. M. Ferdowsi, with the Missouri University of Science and Technology. She completed an internship with The Dow Chemical Company, Houston, TX, in the summer of 2007. Since January 2008, she has been an electrical engineer with the Engineering Solutions, The Dow Chemical Company.

Mehdi Ferdowsi (M'04) received the B.Sc. degree from the University of Tehran, Tehran, Iran, in 1997.

He is currently an Assistant Professor of electrical and computer engineering with the Department of Electrical and Computer Engineering, Missouri University of Science and Technology (Missouri S&T), Rolla. His research interests include energy storage systems, multiple-input power electronic converters, projected cross point control, and plug-in hybrid electric vehicles.

Dr. Ferdowsi is an Associate Editor for the IEEE TRANSACTIONS ON POWER ELECTRONICS. He was the recipient of Missouri S&T's Outstanding Teaching Award in 2006 and the National Science Foundation CAREER Award in 2007.